Hindawi
Advances in Civil Engineering
Volume 2018, Article ID 9545480, 7 pages
https://doi.org/10.1155/2018/9545480

Research Article

Experimental Study on In-Plane Seismic Performance of Reinforced Brick Walls Bonded with Mud

Hui Wang, Jian-jun Chang, Shi-qin He, and Qing-lei Zhang

North China University of Technology, Beijing 100144, China

Correspondence should be addressed to Shi-qin He; heshiqin@ncut.edu.cn

Received 26 September 2017; Revised 9 February 2018; Accepted 12 April 2018; Published 6 May 2018

Academic Editor: Pier Paolo Rossi

Low-cyclic loading tests were carried on brick walls bonded with mud reinforced by three methods: packing belts, one-side steel-meshed cement mortar, and double-side steel-meshed cement mortar. The failure modes, hysteresis curves of the load-displacement, skeleton curves, and ductility were obtained. The results showed that the bearing capacity of the brick walls bonded with mud reinforced by the abovementioned three methods had been increased to 1.4, 1.7, and 2.2 times as much as that of the unreinforced brick walls, respectively, and the ductility of the reinforced brick walls had been increased to 4.7, 2.1 and 2.2 times, respectively. The integrity and ductility of the reinforced brick walls were effectively improved in different degrees. The experimental results provided specific seismic strengthening techniques for the farmhouses built with brick walls bonded with mud.

1. Introduction

Masonry structure is one of the main structural styles in China [1–3]. In the vast rural areas, there are many masonry structure houses with brick walls bonded with mud. They are dangerous in the earthquake prone areas. The brick building cannot satisfy the requirements of seismic performance. They need to be reinforced immediately.

The seismic performance of full-scale single-room masonry buildings of different typologies under cyclic loading in quasi-static manner had been studied in India [4]. Saleem [5] focused on the seismic performance of fiber-reinforced polymer (FRP) retrofitted buildings with openings at different FRP reinforcement levels. The behaviors of seven one-half scale masonry specimens before and after retrofitting using fiber-reinforced polymer (FRP) were also investigated [6]. A technically feasible and economically affordable PP-band (polypropylene band) retrofitting for low earthquake-resistant masonry structures in developing countries was studied by Sathiparan [7]. The in-plane seismic behavior of ordinary and the retrofitted brick flat arch diaphragms were experimentally investigated by Shakib [8]. The performance of a full-scale single-story confined masonry building was investigated by subjecting it to quasi-static cyclic loading. It was found that the lateral stiffness, lateral load, and deformation capacity of the retrofitted building were improved, whereas the ductility decreased slightly [9, 10]. At present, only one research on the seismic performance of brick wall bonded with mud was carried out, and the method of improving the lateral stiffness of the front vertical wall was put forward [11].

In this paper, three seismic strengthening techniques have been applied to the brick walls bonded with mud. The seismic performance, such as the bearing capacity, ductility, and energy dissipation, was obtained by low-cyclic loading tests carried out on brick walls bonded with mud reinforced by packing belts, one-side steel-meshed cement mortar, and double-side steel-meshed cement mortar, respectively. The results could provide an instructive advice in the project of seismic strengthening of farmhouses in rural areas in China.

2. Test Overview

2.1. Design and Manufacture of Specimen. The sizes and forms of the test specimens are shown in Table 1 and Figure 1. In order to ensure no slipping occurs between the

Table 1: Sizes of specimens and reinforcement schemes.

Number		Size (mm)	Reinforcement scheme
Wall specimen	1	$1800 \times 1300 \times 240$	No reinforcement
	2		Angle steels and packing belts
	3		Single-side steel-meshed cement mortar
	4		Double-side steel-meshed cement mortar
Concrete foundation		$4300 \times 500 \times 200$	

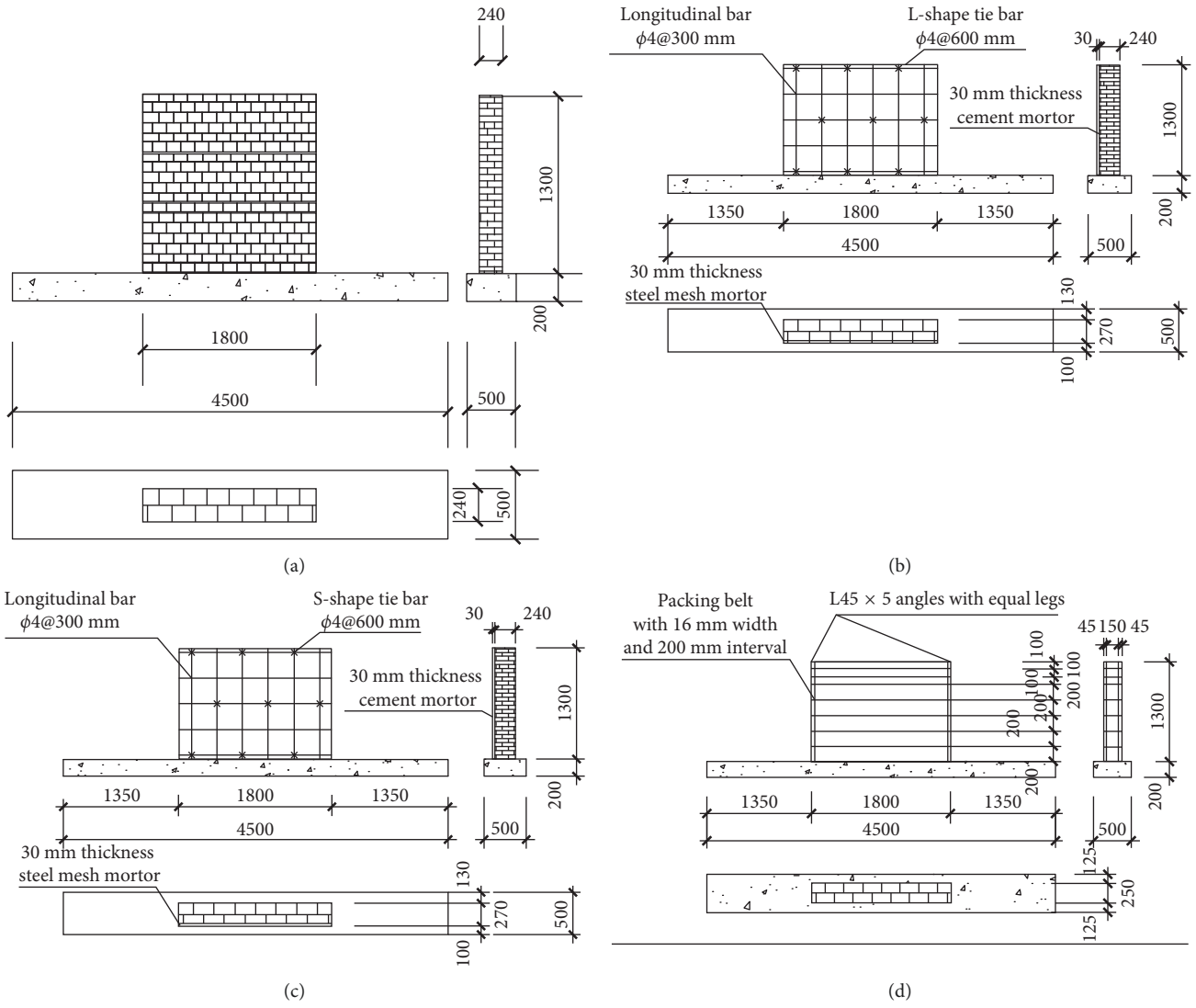

Figure 1: The forms of specimens: (a) specimen #1; (b) specimen #2; (c) specimen #3; (d) specimen #4.

brick walls and the foundations during the tests, the surfaces of the foundations were roughened and the cement mortar was used to cohere the first layer of bricks and the foundations. Then, the walls were built with bricks bonded with mud (10 mm thick). The mud was mixed with clay and fine sand with a mass ratio of 4 : 1.

Considering the convenience and economy of the construction in rural areas, three methods were proposed to reinforce the brick walls [12, 13]. In the first method, the angle steels and packing belts were adopted. In the second and third method, the steel-meshed cement mortar was used to reinforce the walls [14, 15]. The test scheme was shown in Table 1.

The specimen #1 was the unreinforced prototype. After it was damaged, the first reinforced method was used to retrofit the specimen #1, the new one was named specimen #2. In this method, cement mortar was used to fill the cracks of the damaged part of the wall, and four angle steels of $L45 \times 5$ were stuck on the four vertical corners of the wall by cement mortar. Then, the wall was hooped by the packing

Table 2: The strength of the materials.

Materials/size	Specimen #1	Specimen #2	Specimen #3	Specimen #4
Mud test block (MPa) 100 mm ∗ 100 mm ∗ 100 mm	0.43	Same as the specimen #1	0.40	0.41
Clay brick (MPa) 240 mm ∗ 115 mm ∗ 53 mm	4.3		4.8	4.6
Mortar test block (MPa) 70.7 mm ∗ 70.7 mm ∗ 70.7 mm			8.1	8.4
Packing belt (MPa) 16 mm ∗ 0.8 mm		340.3		

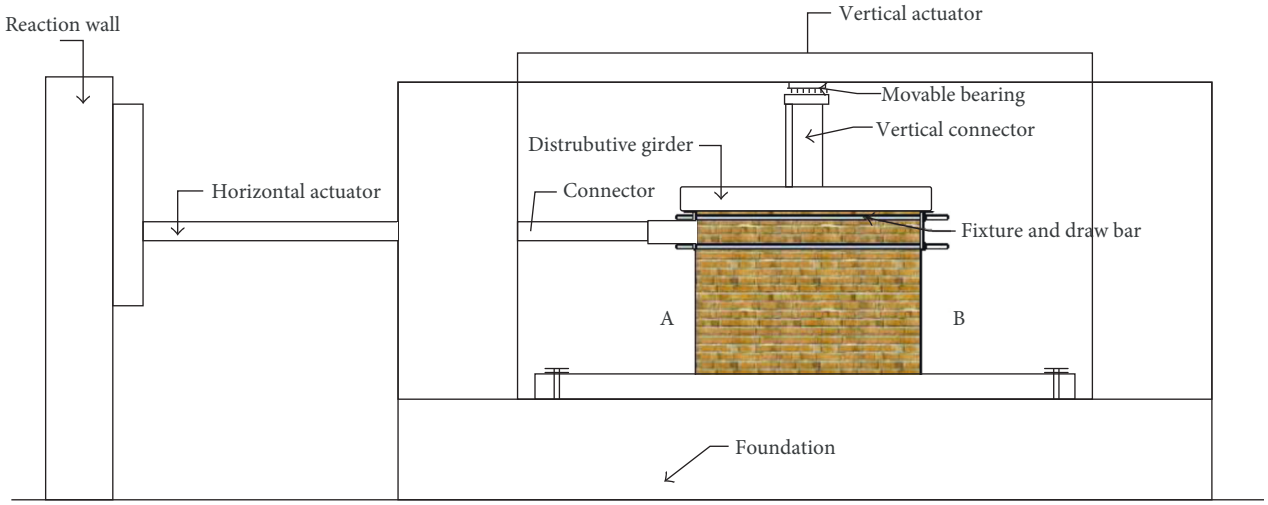

Figure 2: Diagram of experimental equipment.

belts which were 16 mm in width, and the vertical spacing between the belts was 200 mm. The specimen #3 and specimen #4 were reinforced using the steel-meshed cement mortar. For the specimen #3, the wall was reinforced by the steel-meshed cement mortar (30 mm thick) on one side, the diameter of the steel bar was 4 mm, the spacing distance was 300 mm, and the steel mesh was connected with the wall by L-type tensile bar. For the specimen #4, the wall was reinforced by the steel-meshed cement mortar on both sides, and the S-type tensile bar was used to fasten the steel mesh. The parameters of the steel mesh were as same as the specimen #3. The strength of materials is shown in Table 2.

2.2. Loading Mode. A low-cyclic loading mode was applied in the tests. The vertical load including the dead load and live load of the roof was kept at 40 kN during the whole tests, and the axial compression ratio was 0.1. The horizontal loading was controlled by the displacement. The increment of displacement was 0.5 mm at the beginning, and it was added to 1 mm after the crack appeared. The tests were finished when the specimens were damaged or the horizontal force dropped by 15% of the peak value.

The loading device is shown in Figure 2. The horizontal and vertical displacements of the wall, the strain of the angle steels and the packing belts in specimen #2, and the strain of the mortar layer in specimens #3 and #4 were recorded by a high-speed static sample system.

2.3. Test Phenomenon. In order to describe the failure process of every specimen, the loading bearing surface was defined as surface A, and the other side of the wall was defined as surface B (Figure 2). The failure pattern of each specimen is shown in Figure 3.

For the specimen #1, no visible cracks appeared on the wall when the controlling displacement reached ±2 mm. When the displacement increased to ±3 mm, there were small cracks that appeared on the bottom and middle part of the wall. After the displacement reached ±4 mm, the cracks continuously extended. When the displacement increased to ±5 mm, the diagonal through cracks on the wall appeared. The maximum crack was 4 mm in width. At the same time, the specimen was seriously damaged, and the test finished.

For the specimen #2, there were no visible cracks on the wall when the controlling displacement reached ±2 mm. When the displacement increased to ±3 mm, the mended cracks cracked again. After the displacement reached ±4 mm, the diagonal cracks were widened and the vertical cracks appeared near the angle steel. When the displacement reached ±16 mm, the cracks continuously expanded and the bricks were crushed near the sides A and B. When the loading displacement reached ±24 mm, the maximum slip between the wall and the foundation was 10 mm, and the four angle steel was forced to dome outwards. The mud on the middle of the wall fell off, and the wall was damaged seriously. The test finished.

Figure 3: Failure modes of specimens: (a) specimen #1; (b) specimen #2; (c) specimen #3; (d) specimen #4.

For the specimen #3, there were no visible cracks on the wall when the controlling displacement reached ±3 mm. When the displacement increased to ±4 mm, tiny cracks appeared at the root of the wall and the mortar surface. When the displacement increased from ±5 mm to ±13 mm, new cracks appeared near the root of the sides A and B, and the width of the existing cracks became larger. The brick wall began to slip on the foundation. When the displacement reached ±14 mm, the mortar surface near the root of sides A and B was separated from the wall. The load dropped by more than 15% of the peak value. The test finished.

For the specimen #4, no visible cracks appeared on the wall before the controlling displacement reached ±4 mm. When the displacement reached ±5 mm, there were slight cracks that appeared on both sides of the wall. When the displacement increased from ±6 mm to ±18 mm, new cracks appeared on the mortar surface of the sides A and B, and the existing cracks continuously expanded. When the displacement reached ±19 mm, the surface of the mortar was separated from the wall near the root of the sides A and B. The steel bars were exposed, and the load dropped by more than 15% of the peak value. The test finished.

3. Test Results and Analysis

3.1. Analysis of the Hysteretic Curve. The hysteresis curves of each specimen were shown in Figure 4. The crossing cracks were presented on the damaged specimen #1 and specimen #2. After the diagonal crack occurred, the hysteresis curve of the specimen #2 gradually enlarged and the stiffness of the

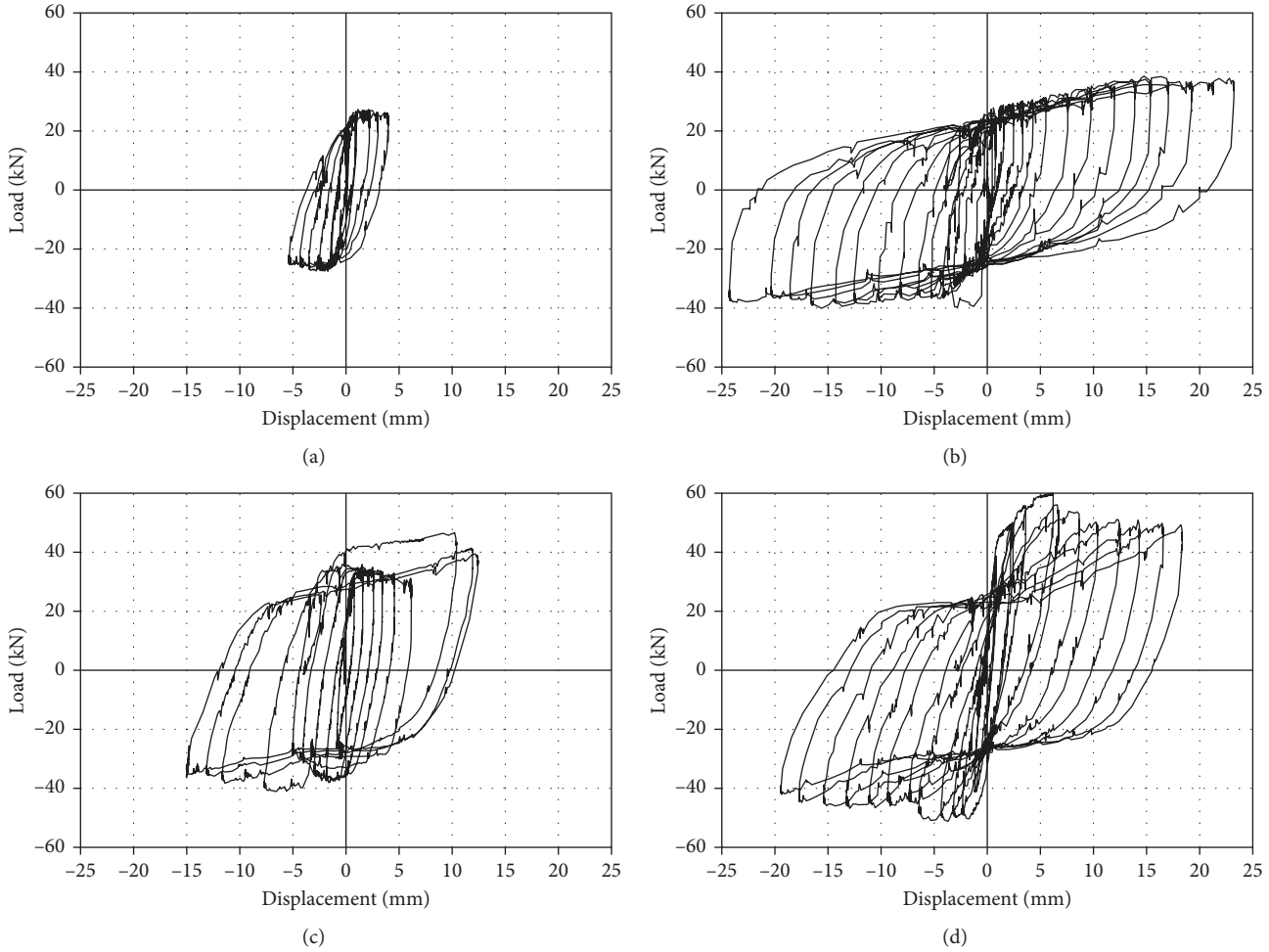

Figure 4: Hysteresis curves of the specimens: (a) specimen #1; (b) specimen #2; (c) specimen #3; (d) specimen #4.

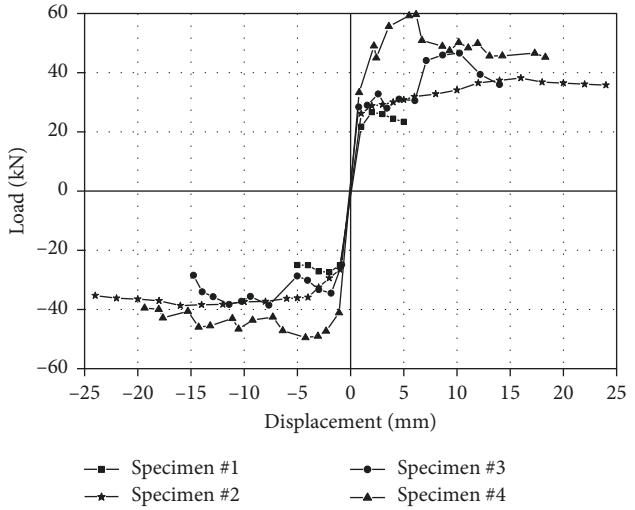

Figure 5: Comparison of skeleton curves.

wall decreased with the increasing displacement. The characteristics of flexural and shear failure were shown in specimen #3 and specimen #4. The initial stage of the hysteresis curve had a spindle shape. With the increasing of shear force and the expanding of the crack, the curve showed the pinching effect due to the degeneration of the stiffness. The area of the hysteretic loop curves indicated the different seismic energy dissipation ability of the specimens. Calculation showed that energy dissipation ability of the specimens #2, #3, and #4 was about 8, 5, and 9 times as much as that of the specimen #1, respectively.

3.2. Analysis of Skeleton Curves. The skeleton curves of each specimen are shown in Figure 5. At the beginning of the tests, the skeleton curves of each specimen were in straight line before the cracking occurred. The slopes of the curves were different which indicated that the lateral stiffness of the walls is different. The maximum bearing capacity of the reinforced specimens was much larger than that of the unreinforced one by comparing the peak point of the skeleton curves. The values are given in Table 2. The positive and negative ultimate bearing capacity of specimen #2, specimen #3, and specimen #4 were increased by 43%, 41%; 70%, 40%; and 124%, 70%; respectively. At the same time, the decline part of the skeleton curve showed that the deformation capacity of the reinforced specimens was improved. The ultimate displacement of

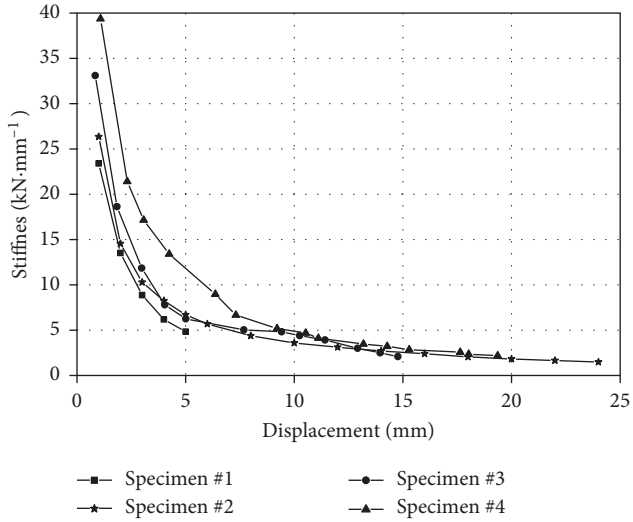

Figure 6: Comparison of stiffness degradation of specimens.

Table 3: Ultimate bearing capacity and ductility coefficients of specimens.

Specimen number	Ultimate bearing capacity (kN)		Cracking displacement (mm)	Failure displacement (mm)	Ductility coefficient
	Positive	Negative			
#1	26.66	−27.4	3	5	1.7
#2	38.2	−38.7	3	24	8
#3	46.62	−38.56	4	14	3.5
#4	59.63	−46.61	5	19	3.8

specimens #2, #3, and #4 were 4.8, 2.80, and 3.85 times that of the specimen #1 when the failure occurred.

3.3. Analysis of Stiffness Degradation. The stiffness of the wall decreased with the increasing number of the loading cycles and the controlling horizontal displacement. The phenomenon was called the stiffness degradation, which indicated the accumulated damage in the walls. The in-plane stiffness of the wall was defined as

$$K_i = \frac{\left|P_i^+\right| + \left|P_i^-\right|}{\Delta_i^+ + \Delta_i^-}, \quad (1)$$

where P_i is the peak load in the i cycle, and Δ_i is the horizontal displacement in the i cycle.

Base on formula (1), the stiffness degeneration curves of each specimen were calculated. There were three stages during the stiffness degradation of the specimens (Figure 6). At the beginning, the initial cracks on the wall gradually formed, the stiffness curve decreased steeply, and the stiffness degenerated sharply. With the extension of the cracks, the speed of the stiffness decline slowed down. After the main cracks appeared, the residual stiffness of the specimen almost remained constant. The differences of the stiffness degeneration among the specimens are shown in Figure 6.

3.4. Ductility Analysis. Ductility reflects the seismic performance of the structure. It is the nonlinear deformation capacity of the structure or component without significant reduction of the bearing capacity. Normally, the ductility coefficient is the ratio of the failure displacement and the yield displacement. However, it is difficult to determine the yield displacement for the masonry structure. The yield displacement was replaced by the cracking displacement. The ductility coefficient μ was calculated by formula (2), and the results are listed in Table 3.

$$\mu = \frac{\Delta_u}{\Delta_{cr}}, \quad (2)$$

where Δ_u is the failure displacement of the specimen, and Δ_{cr} is the crack displacement.

It could be found that the cracks appeared when displacement was small, but the failure displacement of the specimens #2, #3, and #4 can reach 24 mm, 14 mm, and 19 mm, respectively, and the ductility coefficients were 4.7, 2.1, and 2.2 times that of specimen #1. The seismic behavior and bearing capacity of the reinforced specimens #2, #3, and #4 were improved in different degrees. The reinforced methods, packing belts, one-side steel-meshed cement mortar, and double-side steel-meshed cement mortar, proposed in this paper were practicable.

4. Conclusions

Low-cyclic loading tests were carried on the brick walls reinforced by packing belt, single-side steel-meshed cement mortar, and double-side steel-meshed cement mortar. The energy

dissipation performance, bearing capacity, and displacement of the reinforced specimens were discussed and compared to the unreinforced specimen. The main conclusions are as follows:

(1) The bearing and deformation capacity of the reinforced specimens were improved. The bearing capacity and the ductility of the specimen #2 reinforced by packing belts increased to 1.4 and 4.7 times that of the unreinforced specimen #1. The bearing capacity and the ductility of the specimen #3 reinforced by one-side steel-meshed cement mortar increased to 1.7 and 2.1 times that of the unreinforced specimen #1. The bearing capacity and the ductility of the specimen #4 reinforced by double-side steel-meshed cement mortar increased to 2.2 and 2.2 times that of the unreinforced specimen #1. The results indicated that the deformation capacity was greatly enhanced.

(2) After reinforced by steel-meshed cement mortar, there were no cracks that appeared in the middle part of the specimens #3 and #4. A good composite effect between the brick wall and the cement mortar layer was shown before the specimens were destroyed. Although the stiffness of the wall reinforced by the packing belts was increased slightly, it showed a good integrity due to the confined effect of the packing belts.

(3) The seismic performance of the brick walls bonded with mud reinforced by packing belts, one-side steel-meshed cement mortar, and double-side steel-meshed cement mortar was improved greatly. It is noteworthy that the seismic performance depends on not only the component but also the integrity of the structure. Most of the rural houses in China are single-store structures with poor integrality. When the rural houses are strengthened, reinforcing the wall and strengthening the integrity of the structure should be considered at the same time, and the convenience and economy should also be taken into account.

Conflicts of Interest

The authors declare that there are no conflicts of interest regarding the publication of this paper.

Acknowledgments

The research work is supported by the General Program of Science and Technology Development Project of Beijing Municipal Education Commission (Grant no. KM201710009009).

References

[1] Q. F. Xu, H. C. Jiang, L. Zhu et al., "Experimental study on reinforced concrete brick wall strengthened by Ferrocement," *China Civil Engineering Journal*, vol. 42, no. 4, pp. 77–83, 2009.

[2] H. J. Xiao and W. D. Liu, "Experiment of the existing capacity of masonry blocks of in-service historical preserved buildings," *Architectural Structure*, vol. 40, no. 11, pp. 112–114, 2010.

[3] J. Hao, *Experimental Study on Earthquake Resistant Behavior of Mud Bonded Brick Wall with Opening*, Beijing Jiaotong University, Beijing, China, 2010.

[4] A. Chourasia, S. K. Bhattacharyya, and N. M. Bhandari, "Seismic performance of different masonry buildings: full-scale experimental study," *Journal of Performance of Constructed Facilities*, vol. 30, no. 5, 2016.

[5] M. U. Saleem, M. Numada, M. N. Amin, and K. Meguro, "Shake table tests on FRP retrofitted masonry building models," *Journal of Composites for Construction*, vol. 20, no. 5, p. 04016031, 2016.

[6] M. A. ElGawady, P. Lestuzzi, and M. Badoux, "Static cyclic response of masonry walls retrofitted with fiber-reinforced polymers," *Journal of Composites for Construction*, vol. 11, no. 1, pp. 50–61, 2007.

[7] N. Sathiparan and K. Meguro, "Seismic behavior of low earthquake-resistant arch-shaped roof masonry houses retrofitted by PP-band meshes," *Practice Periodical on Structural Design and Construction*, vol. 17, no. 2, pp. 54–64, 2012.

[8] H. Shakib, A. Mirjalili, S. Dardaei, and A. Mazroei, "Experimental investigation of the seismic performance of retrofitted masonry flat arch diaphragms," *Journal of Performance of Constructed Facilities*, vol. 29, no. 4, 2015.

[9] K. Shahzada, A. N. Khan, A. S. Elnashai, A. Naseer, M. Javed, and M. Ashraf, "Shake table test of confined brick masonry building," *Advanced Materials Research*, vol. 5, pp. 689–693, 2011.

[10] D. Silveira, H. Varum, and A. Costa, "Influence of the testing procedures in the mechanical characterization of adobe bricks," *Construction and Building Material*, vol. 40, pp. 719–728, 2013.

[11] M. Li and Z. H. Wang, "Experimental study on low strength brick masonry strengthened with ferrocement," *Architectural Structure*, vol. 33, no. 10, pp. 34–36, 2003.

[12] G. Z. Zeng, B. H. Li, F. Q. Xu et al., "Experimental study on seismic performance of steel reinforcement and packaged with low strength brick," *Engineering Earthquake Resistance and Reinforcement and Reconstruction*, vol. 33, no. 6, pp. 58–62, 2011.

[13] M. Taghdi, M. Bruneau, and M. Saatcioglu, "Seismic retrofitting of 1ow-rise masonry and concrete walls using steel strips," *Journal of Structural Engineering*, vol. 9, pp. 1105–1107, 2000.

[14] S. M. Ali Shah, K. Shahzada, and B. Gencturk, "Retrofitting of full-scale confined masonry building using ferro-cement overlay," *Journal of Performance of Constructed Facilities*, vol. 31, no. 5, 2017.

[15] H. Shakib, S. Dardaei, M. Mousavi, and M. K. Rezaei, "Experimental and analytical evaluation of confined masonry walls retrofitted with CFRP strips and mesh-reinforced PF shotcrete," *Journal of Performance of Constructe Facilities*, vol. 30, no. 6, 2016.